Supporting Information

A VUV Photoionization Study on the Formation of the Simplest Polycyclic Aromatic Hydrocarbon: Naphthalene ($C_{10}H_8$)

Long Zhao, Ralf I. Kaiser*,[1]

Department of Chemistry, University of Hawaii at Manoa, Honolulu, Hawaii, 96822

Bo Xu, Utuq Ablikim, Musahid Ahmed*,[2]

Chemical Sciences Division, Lawrence Berkeley National Laboratory, Berkeley, California 94720

Marsel V. Zagidullin and Valeriy N. Azyazov

Samara National Research University, Samara 443086, Russia and

Lebedev Physical Institute, Samara 443011, Russia

A. Hasan Howlader and Stanislaw F. Wnuk

Department of Chemistry and Biochemistry, Florida International University, Miami, Florida 33199

Alexander M. Mebel*,[3]

Department of Chemistry and Biochemistry, Florida International University, Miami, Florida 33199 and Samara National Research University, Samara 443086

[1] E-mail: ralfk@hawaii.edu
[2] E-mail: mahmed@lbl.gov
[3] E-mail: mebela@fiu.edu

1. Synthesis of 4-phenylvinylacetylene (P3) and *trans*-1-phenylvinylacetylene (P2)

The 4-phenylvinylacetylene (**P3**) was synthesized by CuI/$Pd(PPh_3)_4$-mediated Sonogashira coupling between phenylacetylene and vinyl bromide in 83% yield. The *trans*-1-phenylvinylacetylene (**P2**) was prepared by CuI/$Pd(PPh_3)_2Cl_2$ coupling between β-bromostyrene and (trimethylsilyl)acetylene followed by desilylation in 95% yield.

General information

^{1}H (400 MHz) and ^{13}C (100.6 MHz) NMR spectra were recorded at ambient temperature in solution of $CDCl_3$. Reaction progress was monitored by TLC on Merck Kieselgel 60-F_{254} sheets with product detection by 254-nm light. Products were purified by column chromatography using Merck Kiselgel 60 (230-400 mesh). Reagent grade chemicals were used and solvents were dried by reflux and distillation from CaH_2 under N_2 unless otherwise specified.

4-Phenylvinylacetylene (But-3-en-1-yn-1-ylbenzene); P3.

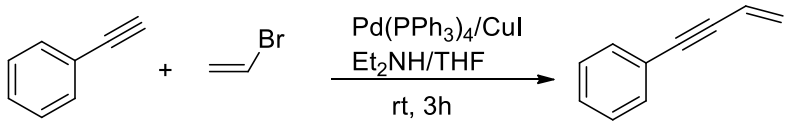

P3

$Pd(PPh_3)_4$ (11.6 mg, 0.01 mmol) and Cu(I)I (7.6 mg, 0.04 mmol) were placed in the flame-dried flask under N_2 at 0 ^oC (ice-bath). Then Et_2NH (1 mL, 707 mg, 9.67 mmol) followed by phenylacetylene (220 µL, 204 mg, 2.0 mmol) and vinyl bromide (2.6 mL; 1.0 M in THF, 2.6 mmol) were added and the resulting mixture was allowed to warm up to ambient temperature and was stirred for 3h [progress of the reaction was monitored by TLC (hexane)]. The reaction mixture was partitioned between water (5 mL) and *iso*pentane/diethyl ether (5 mL; 1:1, v/v). The organic layer was separated and the aqueous layer was extracted with *iso*pentane/diethyl ether twice. The combined organic layer was washed with 1 M HCl, dried (Na_2SO_4) and carefully evaporated (below 30 ^{o}C). The residue was column chromatographed (*n*-hexane) to give **P3**[1] (212 mg, 83%) as colorless liquid: ^{1}H NMR: ($CDCl_3$, 400 MHz) δ 5.55 (dd, J = 11.2, 2.0 Hz, 1H); 5.74 (dd, J = 17.6, 2.0 Hz, 1H); 6.03 (dd, J = 17.6, 11.2 Hz, 1H); 7.32-7.30 (m, 3H); 7.47-7.33 (m, 2H); ^{13}C NMR ($CDCl_3$, 100.6 MHz): δ 88.22, 90.10, 117.32, 123.28, 127.04, 128.40, 128.46, 128.52, 131.63, 131.80.

***trans*-1-phenylvinylacetylene (1-Buten-3-yn-1-ylbenzene); P2.**

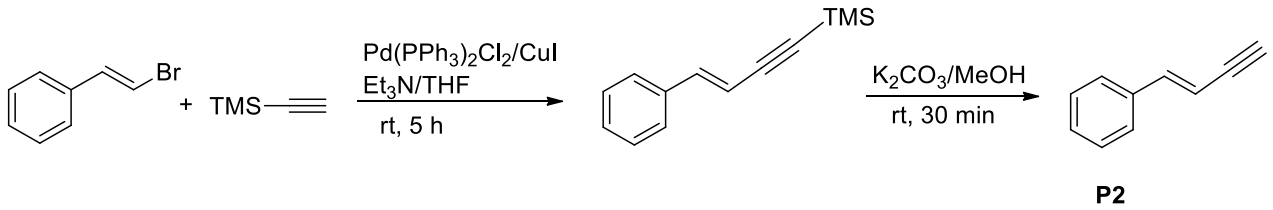

Step a. $Pd(PPh_3)_2Cl_2$ (10.9 mg, 0.016 mmol) and Cu(I)I (5.9 mg, 0.031 mmol) were added to dry THF (5 mL) flame-dried round bottom flask equipped with a stir bar under N_2. Then β-bromostyrene (100 µL, 142 mg, 0.78 mmol) was added followed by TMS-acetylene (161.3 µL, 114 mg, 1.16 mmol) and Et_3N (216 µL, 157 mg, 1.56 mmol). The resulting mixture was stirred at ambient temperature for 5 h [progress of the reaction was monitored by TLC (*n*-hexane)]. The reaction mixture was then diluted with EtOAc and filtered through a short pad of silica. Volatiles were evaporated and the residue was column chromatographed (*n*-hexane) to give TMS-protected **P2** as colorless liquid (150 mg, 96%): ^{1}H NMR ($CDCl_3$, 400 MHz) δ 0.23 (s, 9H); 6.18 (d, J = 16.4 Hz, 1H); 7.01 (d, J = 16.4 Hz, 1H), 7.28-7.39 (m, 5H). *Step b.* K_2CO_3 (100 mg, 0.72 mmol) was added to a stirred solution of the product from *step a* (145 mg, 0.72 mmol) in MeOH (5.0 mL) at room temperature. After for 30 min, volatiles were evaporated in vacuo and the residue was column chromatographed (*n*-hexane) to give **P2**[2] (91 mg, 99%) as colorless liquid: ^{1}H NMR ($CDCl_3$, 400 MHz) δ 3.06 (d, J = 2.4 Hz, 1H); 6.14 (dd, 16.4, J = 2.4 Hz, 1H); 7.05 (d, J = 16.4 Hz, 1H); 7.30-7.32 (m, 3H); 7.34-7.40 (m, 2H); ^{13}C NMR ($CDCl_3$, 100.6 MHz) δ 79.33, 83.00, 107.13, 126.38, 126.59, 128.96, 136.00, 143.31.

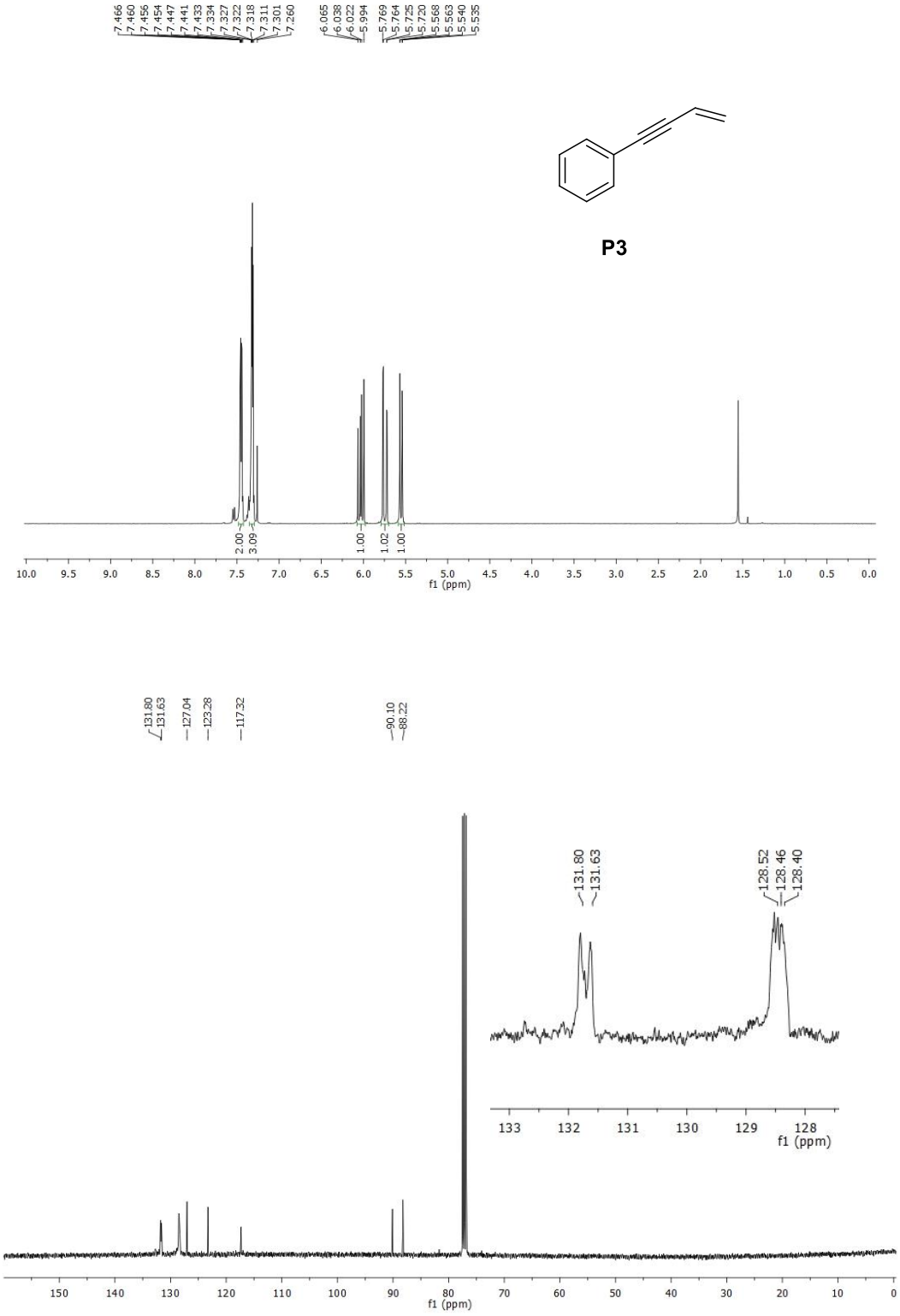

Figure S1. ^{1}H NMR and ^{13}C NMR spectra of compound P3

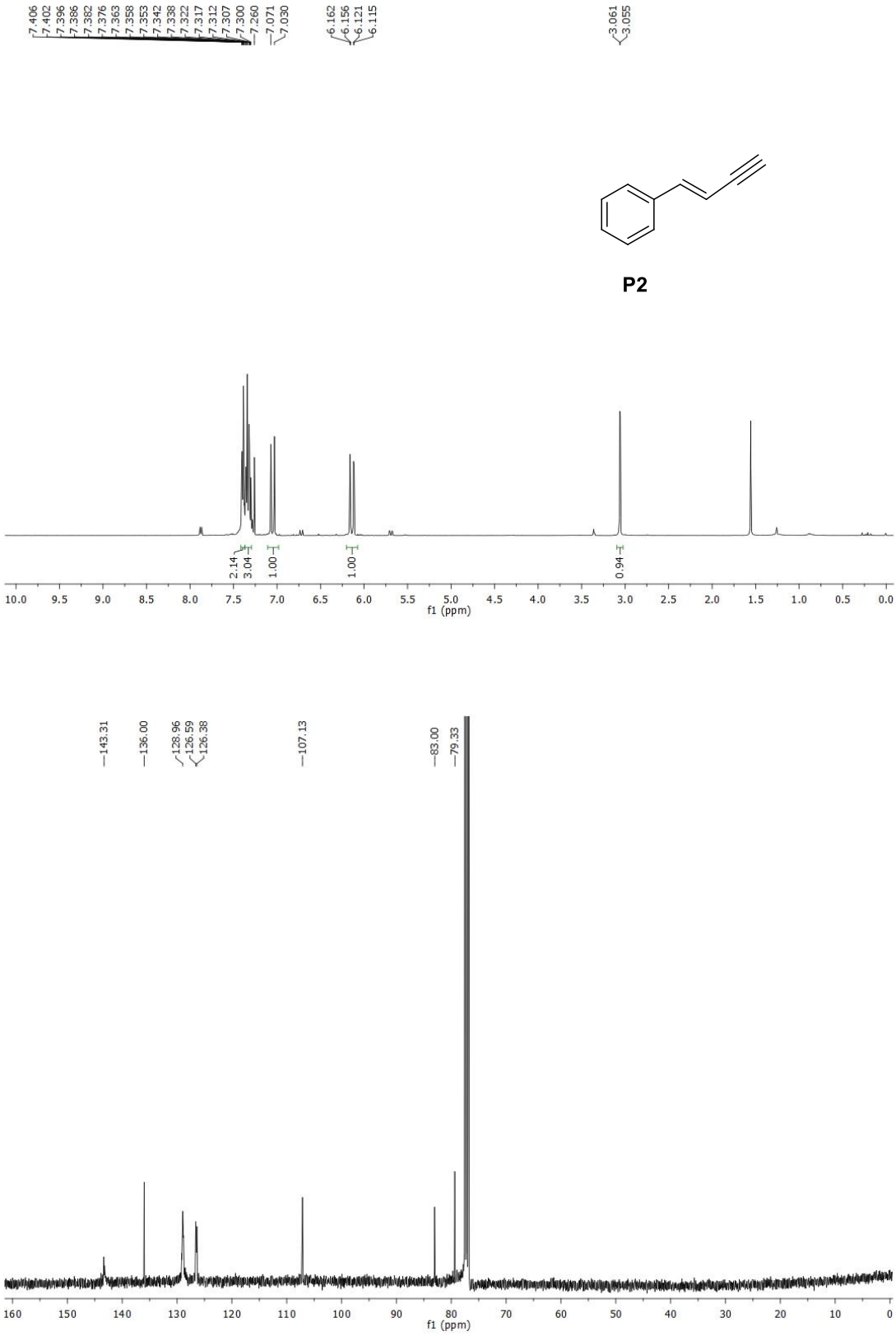

Figure S2. ^{1}H NMR and ^{13}C NMR spectra of compound P2

2. Modeling of the gas flow and kinetics of the phenyl – vinylacetylene system

2.1 Geometry of the task

The axial symmetrical design model of the microreactor is presented in Figure S3 and employed in the COMSOL Multiphysics package.

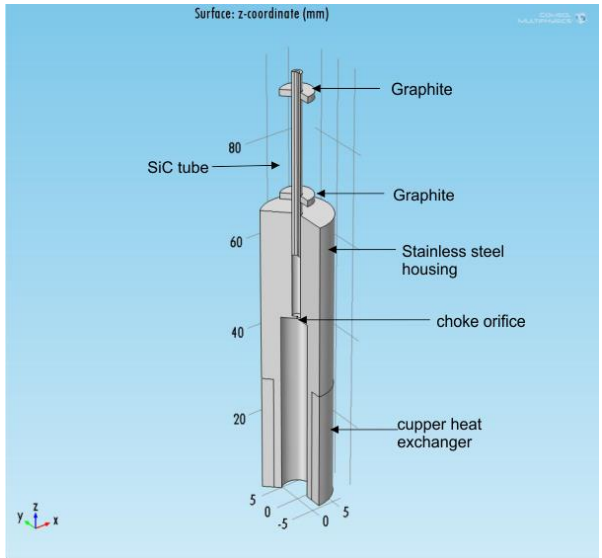

Figure S3. Dimensions of the microreactor in millimeters (mm). The materials and dimensions are compiled in Table S1.

Table S1. Specifications of the main details of the microreactor model.

Part	Size	Material
Graphite reactor	Tube of 2 mm outer diameter, 1 mm inner diameter, 38.1 mm length	SiC
Stainless steel housing	17.6 mm of outer diameter, 62.4 mm of total length. 2 mm internal channel 22.4 mm of length. The inner cylindrical channel 6 mm of diameter, 40 mm of length.	Stainless steel
Heat exchanger	hollow cylinder outer diameter of 17.6 mm, inner diameter of 9.3 mm, length of 25.4 mm	Copper
Graphite Electrodes	Ring 3 mm in thickness, 2 mm of inner diameter, 6.5 mm of outer diameter	Graphite
Choke orifice intended to meter gas flow rate	0.1 mm in diameter, 0.5 mm of thickness	Stainless steel

2.2. Input gas

A gas mixture of C_4H_4 (4.83 ± 0.01%) and He (94.5 ± 0.1 %) along with C_6H_5NO (2.58 ± 0.15 %) was introduced at a temperature of T = 323.0 ± 0.5 K upstream of the choke orifice at an inlet pressure p = 300 Torr upstream of the choke orifice. The maximum temperature is 1,600 K at the SiC microreactor surface. The measured relative fractions of the $C_{10}H_8$ isomers at the exit of the microreactor are presented in Table S2.

Table S2. Relative fractions of the $C_{10}H_8$ isomers at the exit of the microreactor.

Naphthalene	P1	43.5 ± 9.0 %
trans-1-phenylvinylacetylene	P2	6.5 ± 1.0 %
4-phenylvinylacetylene	P3	50 ± 10%
Total		100 %

2.3. Equations

2.3.1. Electric current

The electric potential is employed to the graphite electrodes. The Conductive Media DC COMSOL module was used to solve this problem:

$$-\nabla\left(\left(\frac{1}{rs}\right)\nabla V\right) = 0 \tag{1}$$

Here V is the electric potential, rs is the resistivity depending on temperature. The material physical properties used are shown in Table S3.

2.3.2. Heat transfer

The electric current results in heating of the SiC reactor. The released heat is transferred to stainless steel housing and copper heat exchanger. Another part of released heat is radiative emitted through the outer surface of the set-up. An ideal heat contact between details of the set-up is assumed. The hot inner surface of the SiC reactor heats gas flow in reactor.

The general Heat Transfer module of COMSOL package was used to solve this problem:

For solids:

$$\nabla(\lambda\nabla)\mathrm{T} + \mathrm{Q} = 0 \tag{2}$$

Here, λ is the heat conductivity, Q is the volume heat power. Q = 0 for stainless steel housing and copper heat exchanger. For graphite and the SiC tube resistive heat source is Q = J^2rs, $J = -(\frac{1}{rs})\nabla V$ is the current density, rs is electric resistivity.

For the gas flow, the heat transfer equation applicable for a high Mach number flow was used:

$$C_p\rho(\vec{U}\nabla)T = \nabla(\lambda\nabla)\mathrm{T} + \vec{\tau}:\overrightarrow{S} - \frac{T}{\rho}\frac{\partial\rho}{\partial T}(\vec{U}\nabla)p + Q \tag{3}$$

Here, C_p is the heat capacity per unit mass, ρ is the gas density, U is the gas velocity, $\vec{\tau}:\overrightarrow{S}$ is heat release due to gas viscosity, τ is the viscous stress tensor, $S = 0.5\left(\vec{\nabla}\vec{\mathrm{U}}+\left(\vec{\nabla}\vec{\mathrm{U}}\right)^T\right)$, $\frac{T}{\rho}\frac{\partial\rho}{\partial T}(\vec{U}\nabla)p$ is the heat transformation of kinetic energy to heat. Internal heat power in the gas is negligible in comparison with heat transfer from SiC walls. So, in gas Q = 0. The material physical properties used are shown in Table S3. The boundary

conditions for the heat transfer equations used are listed in Table S4. Heat conductivity of two component gas was calculated using correlation from Reference [3]. The transport properties of pure gases were taken from References [4] and [5].

Table S3. Physical properties of the materials exploited in the microreactor (CGSE system).

SiC	
ρ(g/cm^3)	3.23
C_p(erg/g/K)	$(1.54\times10^6+34790\times T-29.92\times T^2+0.00878\times T^3)$
rs(erg*cm/A^2/s), resistance	$10^7\times(3.6+11.79\times\exp(-(T-300)/608.48))$
ε	0.85
λ, erg/cm/s/K	$10^5\times(40.21+523.43\times\exp(-2.16\times10^{-3}T))$
Graphite	
ρ(g/cm^3)	1.7
C_p(erg/g/K)	2.1391e7-2.5848×exp(-T/492.3)
rs(erg×cm/A^2/s)	$8\times10^3\,(1+0.0002\times(T-300))$
ε	0.7
λ, erg/cm/s/K	4155400+23650000×exp(-0.0021×T)
Stainless steel	
ρ(g/cm^3)	7.9
C_p(erg/g/K)	5×10^6
ε	0.2
λ, erg/cm/s/K	1.254×10^6
Copper	
ρ(g/cm^3)	8.93
C_p(erg/g/K)	3560000+985.5×T
λ, erg/cm/s/K	42400000-7860×T
He	
C_p(erg/g/K)	5.19e7
λ, erg/cm/s/K	100000×10^(-2.2915+0.0349×log10(T)^2+0.51161×log10(T))
μ (g/cm/s)	$10\times(2.858\times10^{-6}$ -1.866e-011×T^2+$6.149\times10^{-8}\times T)$
C_4H_4	
C_p(erg/g/K)	$(-3.43\times10^6+82602\times T-93.61\times T^2+0.0418\times T^3)$
λ, erg/cm/s/K	$1e5\times(8.2\times10^{-3}+5.8647\times10^{-5}\times T+6.3342\times10^{-8}\times T$^2-$2.58\times10^{-11}\times T^3)$
μ (g/cm/s)	$(-11.8158+0.34\times T-1.0362\times10^{-4}\times T^2+1.928\times10^{-8}\times T^3)\times10^{-6}$

Table S4. Boundary conditions for the heat transfer equations.

SiC outer surface	$\varepsilon\sigma(T^4 - T_a^4)$ *
Graphite outer surface	$\varepsilon\sigma(T^4 - T_a^4)$
Stainless steel housing outer surface	$\varepsilon\sigma(T^4 - T_a^4)$
Copper heat exchanger outer surface	T=300K
Internal surface of SiC tube	Continuity of temperature and heat flux
Internal surface of stainless steel housing	Thermal insulation, i.e. temperature of the surface exclusively depends on heat transfer in stainless steel housing
Inner surfaces between materials	Continuity of temperature and heat flux
Gas temperature at the entrance to choke orifice	Equal to the temperature of choke orifice
Gas temperature at the entrance to SiC tube	Gas temperature= temperature at the entrance face of SiC tube
Heat flux at the exit SiC reactor	Convective flux

* ε is the emissivity of the material, T_a = 300 K is the ambient temperature, σ is the Stephan-Boltzmann constant.

2.3.3. Navier-Stocks equation to describe gas motion in the SiC reactor

$$\rho\vec{U}\cdot(\vec{\nabla}\vec{U}) = \vec{\nabla}\left(-pI + \mu\left(\vec{\nabla}\vec{U}+\left(\vec{\nabla}\vec{U}\right)^T\right) - \mu\cdot\frac{2}{3}\vec{\nabla}(\vec{U})I\right) \quad (4)$$

Here p is the gas pressure, μ is the dynamic viscosity, $(\mu\vec{\nabla}\,\vec{U})^T$ is a transposed matrix, I is unit vector. Boundary conditions are listed in Table S5.

Table S5. Boundary conditions for equation (4).

Inlet to SiC tube	p_1 pressure
Outlet from SiC tube	p_2 pressure
Axis of SiC tube	Symmetry $\frac{\partial y}{\partial r} = 0$ for all y
Wall of SiC surface	No slip (U=0)

The viscosity of the two-component He + C_4H_4 gas was calculated using the correlation from Reference S3. A contribution of C_6H_5NO and other products was neglected.

2.4. Mass transfer equations

The concentrations of C_6H_5NO, C_4H_4, and reaction products are much less than the total number density of He. So, we used mass transfer equations for strongly diluted components in the He gas. 18 mass transfer equations were included:

$$\nabla(-D_i\nabla C_i) = R_{Ci} - U\nabla C_i \text{ , i = 1-18} \quad (5)$$

Here C_i is the molar fraction of component i: $C_i=p_i/p$, p_i is the partial pressure of the i-th component, listed in Table S6. In modeling the assumption of strong dilution ($C_i<<1$) is quite important for correction of equation (5). R_{Ci}[fraction/s] is the rate of production of the i-th component. For monomolecular reaction A $\rightarrow$ products, the reaction rate is $R_A = k_A \times C_A$. For bimolecular reaction A + B, the reaction rate is $R_{AB} = k_{AB}C_AC_BN$, where C is molar fraction, N (mol/cm^3) is the total number density. The list of chemical species involved and rate constants of all the reactions (the kinetic package) used are presented in Tables S6 and S7. We implied the following kinetic mechanism:

$C_6H_5NO \leftrightarrows C_6H_5 + NO$	(R1)
$C_4H_4 \rightarrow C_2H_2 + CCH_2/C_2H_2$	(R2)
$C_6H_5 + C_4H_4 \rightarrow$ naphthalene + H	(R3a)
$C_6H_5 + C_4H_4 \rightarrow$ *trans*-1-phenylvinylacetylene + H	(R3b)
$C_6H_5 + C_4H_4 \rightarrow$ 4-phenylvinylacetylene + H	(R3c)
trans-1-phenylvinylacetylene + H $\rightarrow$ naphthalene + H	(R4)
4-phenylvinylacetylene + H $\rightarrow C_6H_5 + C_4H_4$	(R5a)
4-phenylvinylacetylene + H $\rightarrow$ *trans*-1-phenylvinylacetylene + H	(R5b)
4-phenylvinylacetylene + H $\rightarrow$ naphthalene + H	(R5c)
$C_6H_5 + C_2H_2 \rightarrow C_6H_5CCH$ (phenylacetylene) + H	(R6)
$C_4H_4 + H \leftrightarrows C_2H_2 + C_2H_3$	(R7)
$C_2H_3 \leftrightarrows C_2H_2 + H$	(R8)
$C_6H_5 + H \leftrightarrows C_6H_6$ (benzene)	(R9)
C_6H_6 (benzene) + H $\leftrightarrows C_6H_5 + H_2$	(R10)
C_6H_6 (benzene) + H $\leftrightarrows C_6H_6$ (fulvene) + H	(R11)
$C_6H_5 + H \leftrightarrows C_3H_3 + C_3H_3$	(R12)
$C_3H_3 + C_3H_3 \rightarrow C_6H_6$ (benzene)	(R13a)
$C_3H_3 + C_3H_3 \rightarrow C_6H_6$ (fulvene)	(R13b)
$C_3H_3 + C_2H_2 \leftrightarrows$ *c*-C_5H_5	(R14)
$C_6H_5 + C_4H_4 \leftrightarrows$ *i*-C_4H_3/*n*-$C_4H_3 + C_6H_6$	(R15)
$H + C_4H_3 \leftrightarrows C_4H_4$	(R16)
$H + C_4H_4 \leftrightarrows H_2 + C_4H_3$	(R17)
$C_2H_2 + C_4H_3 \rightarrow C_6H_5$	(R18)
$H + C_4H_4 \leftrightarrows C_4H_5$	(R19)
$C_2H_2 + C_4H_5 \rightarrow C_6H_6$ (benzene) + H	(R20a)
$C_2H_2 + C_4H_5 \rightarrow C_6H_6$ (fulvene) + H	(R20b)

Table S6. List of components involved in the reactions in the phenyl – vinylacetylene system.

List of species			
	Formula		Name
1	C_6H_5NO		Nitroso-benzene
2	C_6H_5		Phenyl radical
3	C_4H_4	CH_2=CHCCH	Vinylacetylene (But-1-en-3-yne)
4	C_2H_2	H-C≡C-H	Acetylene
5	$C_{10}H_8$	2 rings	P1, Naphthalene
6	$C_{10}H_8$	C_6H_5-CH=CH-C≡CH	P2
7	$C_{10}H_8$	C_6H_5-C≡C-CH=CH_2	P3
8	H		Atomic hydrogen
9	C_8H_6	C_6H_5-C≡C-H	Phenylacetylene
10	C_2H_3	CH_2=C-H	Vinyl radical
11	C_6H_6		Benzene
12	C_6H_6 (F)	C_5H_4=CH_2	Fulvene
13	H_2		Hydrogen molecule
14	NO		Nitrogen monoxide
15	C_3H_3	HC≡C-CH_2	Propargyl radical
16	c-C_5H_5		Cyclopropadienylidene radical
17	C_4H_3		But-1-en-3-yn-2-yl
18	*i*-C_4H_5	CH_2CHCCH_2	But-1,3-dien-2-yl

Table S7. List of reactions and their nominal rate constants in the phenyl – vinylacetylene system with boundary conditions for equations (5) are listed in Table S8.

	Reaction		Rate constant, $cm^6\ mol^{-2}\ s^{-1}$, $cm^3\ mol^{-1}\ s^{-1}$, or s^{-1}	1,600 K $cm^6\ s^{-1}$, $cm^3\ s^{-1}$, s^{-1}
k_1[6]	$C_6H_5NO \rightarrow C_6H_5 + NO$		1.52e17×exp(-55200/1.987/T)	$4\cdot10^{9}$
k_{1r}[7]	$C_6H_5 + NO \rightarrow C_6H_5NO$		1.03e-11×exp(1940/8.31/T)×6e23	$1.2\cdot10^{-11}$
$k_{2a}p2$[8]	$C_4H_4 \rightarrow C_2H_2 + CCH_2$	7.4 Torr	1.03e71×T^(-16.4)×exp(-121900/1.987/T)+1.46e47×T^(-10.04)×exp(-98810/1.987/T)	98
$k_{2a}p3$[8]	$C_4H_4 \rightarrow C_2H_2 + CCH_2$	74 Torr	3.7e52×T^(-11.68)×exp(-102200/1.987/T)+7.96e62×T^(-13.84)×exp(-118900/1.987/T)	224
k_{2a}	dependent on p		$k_{2a}p2+(k_{2a}p3-k_{2a}p2)/log(10)\times log(p/1333.3/7.4)$	
$k_{2b}p2$[8]	$C_4H_4 \rightarrow C_2H_2 + C_2H_2$	7.4 Torr	4.22e68×T^(-16.04)×exp(-121600/1.987/T)+3.04e43×T^(-9.31)×exp(-98770/1.987/T)	5.7
$k_{2b}p3$[8]	$C_4H_4 \rightarrow C_2H_2 + C_2H_2$	74 Torr	6.18e48×T^(-10.91)×exp(-101100/1.987/T)+3.97e59×T^(-13.18)×exp(-118300/1.987/T)	17
k_{2b}	dependent on p		$k_{2b}p2+(k_{2b}p3-k_{2b}p2)/log(10)\times log(p/1333.3/7.4)$	
k_2			$k_{2a} + k_{2b}$	
k_{3a}[9]	$C_6H_5 + C_4H_4 \rightarrow$ naphthalene + H		3.05e84×T^(-20.96)×exp(-56410/1.987/T)+1.61e32×T^(-5.92)×exp(-26750/1.987/T)	$1.33\cdot10^{-14}$
k_{3b}[9]	$C_6H_5 + C_4H_4 \rightarrow P2 + H$		1.81e69×T^(-16.03)×exp(-48640/1.987/T)+4.18e19×T^(-1.76)×exp(-19320/1.987/T)	$6.7\cdot10^{-13}$
k_{3c}[9]	$C_6H_5 + C_4H_4 \rightarrow P3 + H$		9.34e36×T^(-6.72)×exp(-25850/1.987/T)+4.63e76×T^(-16.56)×exp(-96340/1.987/T)	$1.38\cdot10^{-12}$
k_4[9]	P2 + H → naphthalene + H		9.31e53×T^(-11.45)×exp(-27780/1.987/T)+1.08e35×T^(-6.12)×exp(-13800/1.987/T)	$1\cdot10^{-10}$
k_{5a}[9]	$P3 + H \rightarrow C_6H_5 + C_4H_4$		2.96e44×T^(-8.36)×exp(-35790/1.987/T)+4.64e35×T^(-19.64)×exp(-112800/1.987/T)	$1\cdot10^{-11}$
k_{5b}[9]	P3 + H → P2 + H		1.16e62×T^(-13.64)×exp(-44450/1.987/T)+5.08e83×T^(-18.39)×exp(-99730/1.987/T)	$3.3\cdot10^{-12}$
k_{5c}[9]	P3 + H → naphthalene + H		1.39E+68×T^(-15.84)×exp(-47740/1.987/T)+7.19E+65×T^(-14.12)×exp(-78080/1.987/T)	$1.4\cdot10^{-13}$
k_6[10]	$C_6H_5 + C_2H_2 \rightarrow C_6H_5CCH + H$		3.08e34×T^(-6.06)×exp(-23190/1.987/T)+9.92e55×T^(-11.07)×exp(-	$1.43\cdot10^{-12}$

			70330/1.987/T)	
k_7[11]	C_4H_4+H → C_2H_2+C_2H_3		0.10023e17×T^(-0.47407)×exp(-12128/1.987/T)	$1.1\cdot10^{-11}$
k_{7r}[11]	C_2H_2 + C_2H_3 → H + C_4H_4		0.11184e11×T^0.88224×exp(-6654.1/1.987/T)	$1.5\cdot10^{-12}$
k_8[12]	C_2H_3 → C_2H_2 + H		3.94e12×(T/298)^1.62×exp(-155000/8.3/T)	$5.2\cdot10^{8}$
k_{8r}[13]	C_2H_2 + H + He → C_2H_3 + He		3.31e-30×(6e23)^2×exp(-6150/8.31/T)	$2\cdot10^{-30}$
k_9[14]	C_6H_5 + H → C_6H_6		exp(244.05-34871/T)×T^(-25.9)	$5.7\cdot10^{-11}$
$k_{9r}p1$[15]	C_6H_6 → C_6H_5 + H, p = 30 Torr		1.3489e108×T^(-25.81)×exp(-181750/1.987/T)	4.1
$k_{9r}p2$[15]	C_6H_6 → C_6H_5 + H, p = 50 Torr		6.3095e60×T^(-12.4)×exp(-148070/1.987/T)	7.2
k_{9r}	C_6H_6 → C_6H_5 + H, 30<P<50		$k_{9r}p1+(k_{9r}p2-k_{9r}p1)/(50-30)\times(p/1333.3-30)$	
k_{10}[16]	C_6H_6 + H → C_6H_5 + H_2		4.57e8×T^1.88×exp(-14839/1.987/T)	$7.45\cdot10^{-12}$
k_{10r}[16]	C_6H_5 + H_2 → C_6H_6 + H		1.69e4×T^2.64×exp(-4559/1.987/T)	$1.93\cdot10^{-12}$
k_{11}[17]	C_6H_6 + H → C_6H_6 (F) + H		6.54e25×T^(-2.8332)×exp(-43768/1.987/T)	$9.3\cdot10^{-14}$
k_{11r}[17]	C_6H_6 (F) + H → C_6H_6 + H		1.09e25×T^(-3.0678)×exp(-11761/1.987/T)	$6.7\cdot10^{-11}$
k_{12}[15]	C_6H_5 + H → C_3H_3+ C_3H_3		0.18289e81×T^(-17.827)×exp(-75267/1.987/T)	$1.2\cdot10^{-11}$
k_{12r}[15]	C_3H_3 + C_3H_3 → C_6H_5 + H		(10^30.42×T^(-11.94)×exp(-28973/1.987/T) + 10^10.36×T^(-6.722)×exp(-13799/1.987/T))×6e23	$1.68\cdot10^{-12}$
k_{13a}[15]	C_3H_3 + C_3H_3 → C_6H_6		(10^45.33×T^(-16.73)×exp(-27864/1.987/T) + 10^16.07×T^(-8.819)×exp(-7049/1.987/T))×6e23	$8.9\cdot10^{-13}$
k_{13b}[15]	C_3H_3 + C_3H_3 → C_6H_6 (F)		(10^45.59×T^(-17.02)×exp(-25864/1.987/T) + 10^20.46×T^(-10.31)×exp(-7992/1.987/T))×6e23	$3.5\cdot10^{-13}$
k_{14}[18]	C_3H_3 + C_2H_2 → c-C_5H_5		6e23×5.95e34×T^(-14.2)×exp(-31700/1.987/T)	$8.8\cdot10^{-16}$
k_{14r}[18]	c-C_5H_5 → C_3H_3 + C_2H_2		7.55e99×T^(-24.4)×exp(-128200/1.987/T)	$1.56\cdot10^{4}$
k_{15}[9]	C_6H_5 + C_4H_4 → *n,i*-C_4H_3 + C_6H_6		1.97e2×T^3.08×exp(-4463.1/1.987/T)+3.41e2×T^3.11×exp(-8482.7/1.987/T)	10^{-12}
k_{15r}[9]	*n,i*-C_4H_3 + C_6H_6 → C_6H_5 + C_4H_4		544.12×T^2.8952×exp(-14648/1.987/T)+1936.1×T^3.0032×exp(-8387.1/1.987/T)	10^{-12}
$k_{16}p2$[8]	H + C_4H_3 → C_4H_4	7.5 Torr	8.16E+59×T^(-14.09)×exp(-20770.0/1.987/T) +5.88E+91×T^(-24.70)×exp(-26410.0/1.987/T)	$1.4\cdot10^{-12}$
$k_{16}p3$[8]	H + C_4H_3 → C_4H_4	75 Torr	1.98E+65×T^(-15.12)×exp(-30460.0/1.987/T) +1.14E+56×T^(-13.08)×exp(-16980.0/1.987/T)	$9.25\cdot10^{-12}$
k_{16}	H + C_4H_3 → C_4H_4	7.5<p<75	$(k_{16}p2+(k_{16}p3-k_{16}p2)/(75-7.5)\times(p/1333.3-7.5))$	
$k_{16r}p2$[8]	C_4H_4 → C_4H_3+H	7.5 Torr	1.41E+65×T^(-14.94)×exp(-124900.0/1.987/T) + 2.19E+85×T^(-21.94)×exp(-125400.0/1.987/T)	1.72
$k_{16r}p3$[8]	C_4H_4 → C_4H_3 + H	75 Torr	4.02E+69×T^(-15.72)×exp(-133600.0/1.987/T) + 3.48E+60×T^(-13.79)×exp(-119600.0/1.987/T)	11
k_{16r}[8]	C_4H_4 → C_4H_3 + H	7.5<p<75	$(k_{16r}p2+(k_{16r}p3-k_{16r}p2)/(75-7.5)\times(p/1333.3-7.5))$	
k_{17}[a]	H + C_4H_4 → H_2 + C_4H_3		4.47e8×T^1.88×exp(-14839/1.987/T)	$7.45\cdot10^{-12}$

k_{17r}[b]	$H_2 + C_4H_3 \rightarrow H + C_4H_4$		1.69e4×T^2.64×exp(-4559/1.987/T)	$2\cdot10^{-12}$
k_{18}[19]	$C_2H_2 + C_4H_3 \rightarrow C_6H_5$		3.47e2×6.022e23×(T/298)^(-14.7)×exp(-130000/8.314/T)	$3.7\cdot10^{-13}$
$k_{19}p1$[11]	$H + C_4H_4 \rightarrow$ *i*-C_4H_5	7.5 Torr	0.1091e56×T^(-13.094)×exp(-17169/1.987/T)	$9.1\cdot10^{-14}$
$k_{19}p2$[11]	$H + C_4H_4 \rightarrow$ *i*-C_4H_5	29 Torr	0.88414e53×T^(-12.227)×exp(-17302/1.987/T)	$2.9\cdot10^{-13}$
k_{19}	$H + C_4H_4 \rightarrow$ *i*-C_4H_5	7.5<p<29	$k_{19}p1$+($k_{19}p2$-$k_{19}p1$)×log(p/7.5/1333.3)/log(29/7.4)	
$k_{19r}p1$[11]	*i*-$C_4H_5 \rightarrow H + C_4H_4$	7.5 Torr	0.5996e79×T^(-12.904)×exp(-61076/1.987/T)/6e23	$2.06\cdot10^{5}$
$k_{19r}p2$[11]	*i*-$C_4H_5 \rightarrow H + C_4H_4$	29 Torr	0.16992e78×T^(-12.251)×exp(-61446/1.987/T)/6e23	$6.4\cdot10^{5}$
k_{19r}	*i*-$C_4H_5 \rightarrow H + C_4H_4$	7.5<p<29	($k_{19r}p1$+($k_{19r}p2$-$k_{19r}p1$)×(P/1333.3-7.4)/21.6)	
k_{20a}[20]	C_2H_2 + *i*-$C_4H_5 \rightarrow H + C_6H_6$		1.47e23×T^(-3.28)×exp(-24907/1.987/T)	$3\cdot10^{-15}$
k_{20b}[20]	C_2H_2 + *i*-$C_4H_5 \rightarrow H + C_6H_6$ (F)		6.5e24×T^(-3.44)×exp(-20319/1.987/T)	$1.7\cdot10^{-13}$

Note: a. k_{17} is taken to be the same as k_{10} for $C_6H_6 + H \rightarrow C_6H_5 + H_2$.
b. k_{17r} is taken to be the same as k_{10r} for $C_6H_5 + H_2 \rightarrow C_6H_6 + H$.

Table S8. Boundary conditions for equations (5).

Inlet to SiC tube	Molar fraction of C_i (C_1=0.05, C_3=0.0258, all other C_i=0)
Outlet from SiC tube	Convective flux
Axis of SiC tube	Symmetry $\frac{\partial c_i}{\partial r} = 0$ for all y
Wall of SiC surface	insulation

Diffusion coefficients D_i are presented in Table S9. These values were taken from References S4 and S5 for diffusion in air ambient gas. A simplified correction of these values was made for He ambient gas.

Table S9. Diffusion coefficients D_i.

D_1	(-0.06609+3.4744e-04×T+3.9244e-07)×750×1333.3/p×((1+107/4)/(1+107/29))^0.5	diffusion C_6H_5NO like for $C_6H_5NO_2$
D_2	(-0.07583+4.3076e-4×T+4.6043e-7×T^2)×750×1333.3/p×((1+77/4)/(1+77/29))^0.5	C_6H_5 like for C_6H_6
D_3	(-0.09144+5.29e-4×T+5.44e-7×T^2)×750×1333.3/p×((1+52/4)/(1+52/29))^0.5	C_4H_4
D_4	(-0.13184+8.3257e-4×T+7.64e-7×T^2)×750×1333.3/p×((1+26/4)/(1+26/29))^0.5	C_2H_2
D_5	(-0.04311+2.5699e-4×T+4.185e-7×T^2)×750×1333.3/p×((1+106/4)/(1+106/29))^0.5	$C_{10}H_8$ (P1, naphthalene)
D_6	(-0.04311+2.5699e-4×T+4.185e-7×T^2)×750×1333.3/p×((1+106/4)/(1+106/29))^0.5	$C_{10}H_8$ (P2)
D_7	(-0.04311+2.5699e-4×T+4.185e-7×T^2)×750×1333.3/p×((1+106/4)/(1+106/29))^0.5	$C_{10}H_8$ (P3)
D_8	(-0.16301+1.6882e-3×T+2.27255e-6×T^2)×750×1333.3/p×((1+1/4)/(1+1/29))^0.5	H
D_9	(-0.06739+3.5096e-4×T+4.027e-7×T^2)×750×1333.3/p×((1+102/4)/(1+102/29))^0.5	C_6H_5CCH
D_{10}	(-0.13184+8.3257e-4×T+7.64e-7×T^2)×750×1333.3/p×((1+27/4)/(1+27/29))^0.5	C_2H_3 like for C_2H_2
D_{11}	(-0.07583+4.3076e-4×T+4.6043e-7×T^2)×750×1333.3/p×((1+78/4)/(1+78/29))^0.5	C_6H_6 (benzene)
D_{12}	(-0.07583+4.3076e-4×T+4.6043e-7×T^2)×750×1333.3/p×((1+78/4)/(1+78/29))^0.5	C_6H_6 (F, fulvene)
D_{13}	(-074707+3.73626e-3×T+3.2442e-6×T^2)×750×1333.3/p×((1+2/4)/(1+2/29))^0.5	H_2
D_{14}	(-0.09443+7.8814e-4×T+1.0532e-7×T^2)×750×1333.3/p×((1+30/4)/(1+30/29))^0.5	NO
D_{15}	(-0.11168+6.095e-4×T+6.274e-7×T^2)×750×1333.3/p×((1+39/4)/(1+39/29))^0.5	C_3H_3
D_{16}	(-0.08285+4.71e-4×T+4.9668e-7×T^2)×750×1333.3/p×((1+65/4)/(1+65/29))^0.5	c-C_5H_5
D_{17}	(-0.09144+5.29e-4×T+5.44e-7×T^2)×750×1333.3/p×((1+51/4)/(1+51/29))^0.5	C_4H_3 like for C_4H_4
D18	(-0.08877+5.0649e-4×T+5.2566e-7×T^2)×750×1333.3/p×((1+53/4)/(1+53/29))^0.5	C_4H_5

2.5. Calculated parameters

2.5.1. Temperature of solids

At the electric power of 65 W, a temperature of 1,600 K of SiC tube wall is established at the distance of 2.5 cm downstream from the entrance into the SiC tube. The temperature distribution in the solids is shown in Figure S4. This solution gave a temperature of the choke orifice of 475 K. The temperature of the inlet edge of the SiC tube was determined to be 610 K. This temperature was utilized as the boundary value for the heat transfer problem in the gas flow.

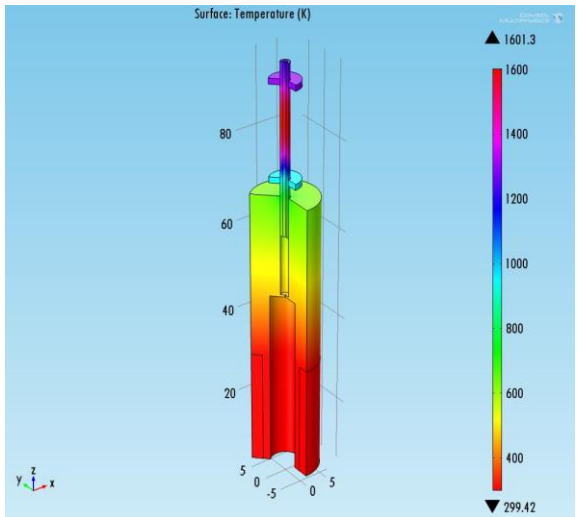

Figure S4. Temperature distribution in the microreactor.

2.5.2. Gas molar and mass flow rate

The gas flow rate is controlled by gas outflow through the choke orifice. The mass gas flow rate was determined according to the formula

$$M_g = \varphi\pi\left(\frac{d_0}{2}\right)^2\sqrt{\gamma\left(\frac{2}{\gamma+1}\right)^{\frac{\gamma+1}{\gamma-1}}}\frac{P_{st}}{\sqrt{R_g T_{st}}}. \quad (6)$$

Here γ is the adiabatic constant, P_{st} = 300 Torr is the gas stagnation pressure upstream choke orifice, d_0 is the diameter of the choke orifice, $R_g(erg/g/K)$ =8.31·10^7/(molecular weight) is the gas constant per unity of the gas mass, T_{st} is the gas stagnation temperature, φ is a discharge coefficient – the efficient relative fraction of the orifice area where the gas velocity equals to the sonic velocity. For thin choke orifice, the discharge coefficient is in the range of φ = 0.8÷0.9. We have assumed φ = 0.85. Assuming T_{st} = 475 K, equation (6) gives the mass flow rate M_g = 2.76×10^{-4} g/s and the molar flow rate M_m = 3.07×10^{-4} mol/s.

2.5.3. Gas flow parameters

The calculated profiles of the axial gas temperature, velocity and pressure are shown in Figure S5. The gas dynamic parameters exhibit strong axial gradients. The strong cooling of the gas flow at the outlet is due to strong radiative cooling of the unheated edge of the SiC tube. At a very short distance of a few mm the gas velocity achieves the speed of the sound. The cross flow profiles of temperature and pressure are almost uniform. The cross flow profile of z-velocity is almost parabolic.

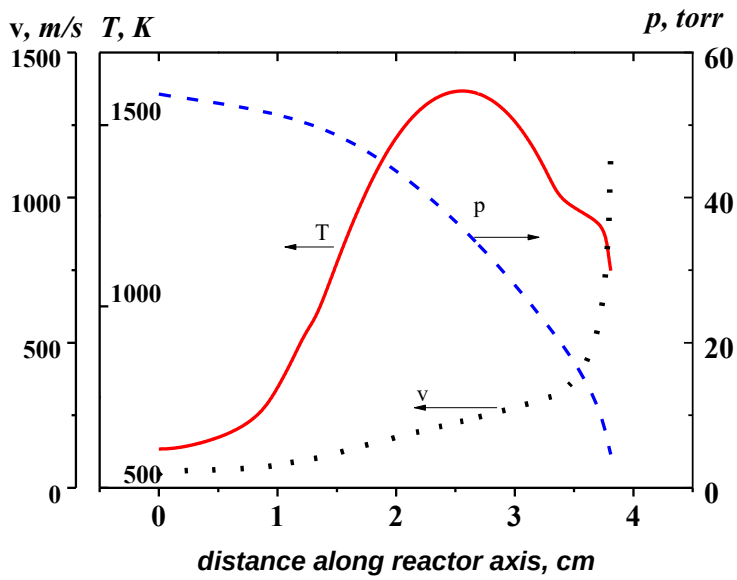

Figure S5. Gas dynamic parameters of the flow in the reactor.

2.5.4. Mole fractions at the exit of the reactor

The output mole "fraction" of a component C_i is calculated by integration

$$G_i = \int_0^{d/2} C_i\, N v * 2\pi r / M_m \qquad (7)$$

N , v, C_i are current number density, axial velocity, mole fraction., M_m is input total molar flow rate of all components (He + C_6H_5NO + C_4H_4). Equation (7) allows us to calculate ratios G_i/G_j for any i and j. For C_1 = 0 (no C_6H_5NO present) calculations gave the efficiency of C_4H_4 decomposition of C_3/C_3^0 = 0.01, which is lower than the measured value of 0.05. The calculated rates of reaction 2 and reaction 7 are shown in Figure S6. Their comparison shows that the H + C_4H_4 → C_2H_2 + C_2H_3 reaction (7) is the prevailing source of acetylene and therefore our simulation results in presence of C_6H_5NO appeared to be insensitive to the rate of unimolecular decomposition of C_4H_4.

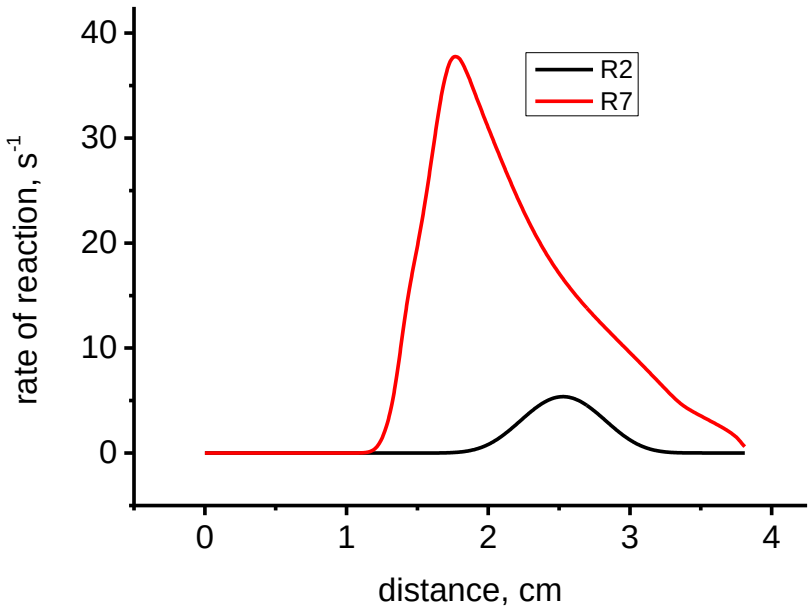

Figure S6. Rate of reactions 2 and 7 with calculated molar fractions of major and minor products shown in Figure S7.

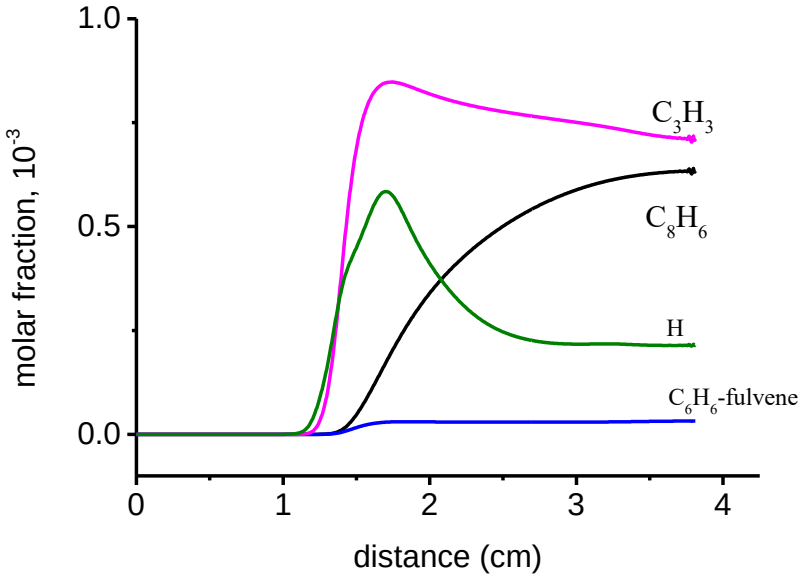

Figure S7. Profiles of the molar fraction of the minor products H, C_6H_6 (fulvene), C_3H_3, and C_8H_6 (phenylacetylene).

2.5.5. Calculation of the gas residence time.

The gas residence time inside distance interval [z,z+L] in SiC tube is defined as:

$$\boldsymbol{t_{res} = \int_{z}^{z+L} dz \int_{0}^{d/2} \frac{2\pi r \rho dr}{M_g}}$$

Here, d is the diameter of the microreactor. The calculations give the t_{res} = 564 μs inside the SiC tube in the interval [0, 3.81 cm] and t_{res}=300 μs inside interval [0,1 cm]. The axial residence time is defined as

$$t_{res}^{a} = \int_{z}^{z+L} \frac{dz}{u_a}$$

Here u_a is the axial gas velocity in the center of the tube. Because of near parabolic velocity profile one has approximately $t_{res}^{a} \approx 0.5 t_{res}$.

2.5.6. Additional details of the reaction mechanisms

The calculated ratios [P2]/[P1] and [P3]/[P1] of ~0.3 and ~2.5 are somewhat out the confidence intervals of the experimental values, 0.12-0.22 and 0.76-1.74, respectively. One of the possible reasons for this discrepancy is that the experimental conditions, in particular, the mass flow rate and SiC tube temperature distribution, are not fully well defined. Our analysis showed that a variation of the mass flow rate through the microreactor by factors 0.5 to 2 does not change the calculation results substantially. A decrease of the SiC heat conductivity by factors 5 to 8 resulted in a more uniform temperature distribution but has not lead to a substantial change of the [P3]/[P1] ratio. Much more significant is the influence of the rate constant values. The calculated rate constants k_3, k_4, and k_5 are expected to have a kinetic accuracy within a factor of 2. A simple decrease of the value of k_{3c} by a factor of 2 results in the calculated values [P3]/[P1] ≈ 1 and [P2]/[P1] ≈ 0.15. Thus, within the error bars of the theoretical calculations of the rate constants, the predicted relative yields of P1, P2, and P3 are in close agreement with the experimental data. The calculations showed that a substantial part (nearly 50%) of C_6H_5 radicals is consumed in the competitive reactions (R6), (R9), (R11), and (R12) producing benzene, fulvene, phenylacetylene, and propargyl. These reactions also consume hydrogen atoms needed for reactions (R4) and (R5).

The kinetic modeling results clearly demonstrate that naphthalene is produced predominantly via secondary reactions of hydrogen-assisted isomerization of the other $C_{10}H_8$ isomers, *trans*-1-phenylvinylacetylene (P2) and 4-phenylacetylene (P3). Naphthalene is the predominant product of the P2 + H reaction with a high rate constant of 1.1×10^{-10} cm^3 $molecule^{-1}$ s^{-1} close to the kinetic limit at 1,600 K and

30 Torr. Here, a hydrogen atom adds to the terminal acetylenic carbon atom of *trans*-1-phenylvinylacetylene producing intermediates [i8] or [i7] via low barriers of 10 and 5 kJmol^{-1}. Next, [i7] easily rearranges to [i8] by rotation around the single C-C bond in the side chain and [i10] features a facile 1,5-H migration to [i11], which in turn undergoes a fast six-member ring closure followed by hydrogen loss giving rise to naphthalene. For the P3 + H reaction, two channels producing C_6H_5 + C_4H_4 and P2 + H are competitive with the respective rate constants of 1.1×10^{-11} and 3.5×10^{-12} cm^3 molecule^{-1} s^{-1}, whereas the formation of naphthalene, 1.4×10^{-13} cm^3 molecule^{-1} s^{-1}, is minor. Therefore, a fraction of the P3 + H reaction flux, which does not restore the initial reactants, converts to P2 + H and P2 then undergoes a fast H-assisted isomerization to naphthalene P1.

The second most abundant product in the present experiment is phenylacetylene, which can be formed in the C_6H_5 + C_2H_2 reaction (R6). Acetylene can in principle originate from unimolecular decomposition of vinylacetylene in the reactor. However, our simulation shows that the H + $C_4H_4 \rightarrow C_2H_2 + C_2H_3$ reaction (R7) is the prevailing source of acetylene. The simulation results appeared to be insensitive to a decrease of the rate constant for the unimolecular decay reaction (R2), which may be even reduced to zero without observing a significant change. Therefore, the initial C_6H_5 + C_4H_4 reaction is essential for the formation of acetylene and then, eventually phenylacetylene, because it rapidly produces H atoms along with $C_{10}H_8$ products. H atoms then react with C_4H_4 forming acetylene. The kinetic mechanism also explains the appearance of the other minor products; here, vinyl radicals C_2H_3 originate from the H + C_4H_4 reaction, C_3H_3 is a minor product of H + C_6H_5, the C_2H_2 + C_3H_3 reaction (R14) produces cyclopentadienyl *c*-C_5H_5, benzene can be formed through the C_6H_5 + H recombination or in the C_4H_5 + C_2H_2 reaction, where C_4H_5 in turn can be produced by H addition to C_4H_4. The C_6H_6 isomers benzene and fulvene can interconvert to one another via H-assisted isomerization.

3. Photoionization efficiency (PIE) curves and fits of low molecular weight products

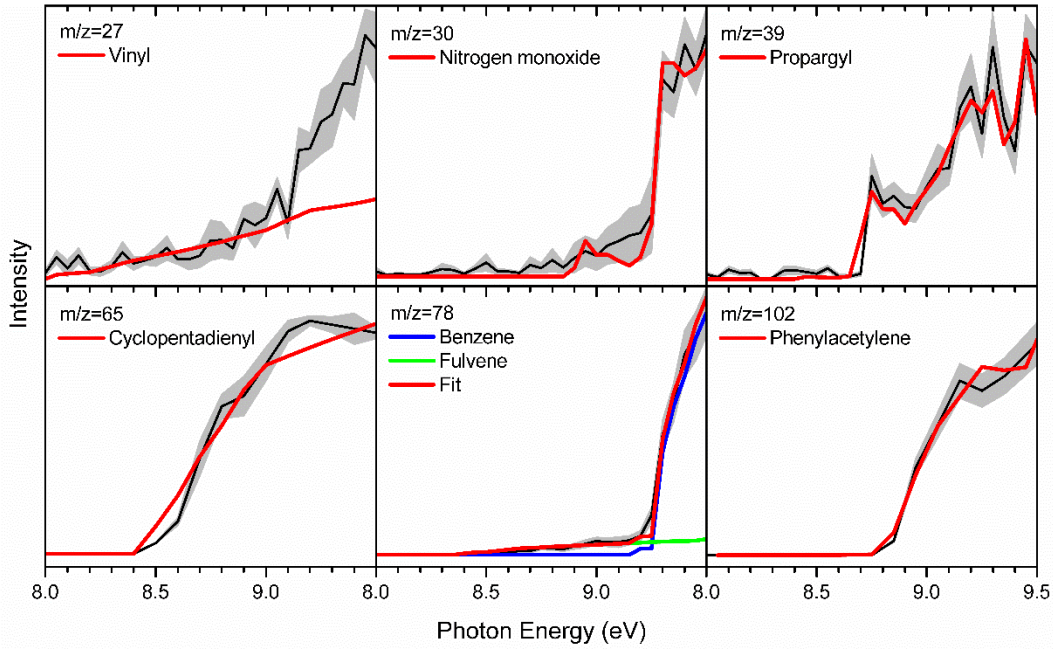

Figure S8. Experimental photoionization efficiency curves (PIE, black lines) recorded in the phenyl-vinylacetylene system for low molecular-weight products along with the experimental errors (gray area) and the reference PIE curves (blue, green and red lines). In case of multiple contributions to one PIE curve, the red line resembles the overall fit. For the fit of m/z = 27, as it may be partially attributed to fragments from high molecular weight species, the fit is not as good as others in the higher energy range.

Table S10. Photoionization information for low molecular weight products.

Species	Structure	m/z	Photoionization energy (eV)	
			Experimental	Ref. 21
C_2H_3 (Vinyl radical)		27	8.20 ± 0.05	8.25
NO (Nitrogen monoxide)		30	8.80 ± 0.05	8.85
C_3H_3 (Propargyl radical)		39	8.70 ± 0.05	8.67
C_5H_5 (Cyclopentadienyl radical)		65	8.40 ± 0.05	8.41
C_6H_6 (fulvene)	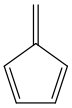	78	8.35 ± 0.05	8.36
C_6H_6 (Benzene)		78	9.20 ± 0.05	9.24
C_8H_6 (Phenylacetylene)	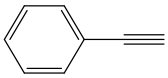	102	8.75 ± 0.05	8.82

References

(1) Nguyen, T. H.; Morris, S. A.; Zheng, N. Intermolecular [3+2] Annulation of Cyclopropylanilines with Alkynes, Enynes, and Diynes via Visible Light Photocatalysis. *Adv. Synth. Catal.* **2014,** *356*, 2831-2837.
(2) Cheng, J.-K.; Loh, T.-P. Copper- and Cobalt-Catalyzed Direct Coupling of sp3 α-Carbon of Alcohols with Alkenes and Hydroperoxides. *J. Am. Chem. Soc.* **2015,** *137*, 42-45.
(3) Reid, R. C.; Prausnitz, J. M.; Sherwood, T. K. *The Properties of Gases and Liquids, Third Edition*; McGraw-Hill; 1977.
(4) Yaws, C. L. *Transport properties of chemicals and hydrocarbons: viscosity, thermal conductivity, and diffusivity of Cl to Cl00 organics and Ac to Zr inorganic*; William Andrew; 2009.
(5) Yaws, C. L. *Transport properties of chemicals and hydrocarbons: Including C1 to C100 Organics and Ac to Zr Inorganics*. William Andrew; 2014.
(6) Park, J.; Dyakov, I. V.; Mebel, A. M.; Lin, M. C. Experimental and Theoretical Studies of the Unimolecular Decomposition of Nitrosobenzene: High-Pressure Rate Constants and the C− N Bond Strength. *J. Phys. Chem. A* **1997,** *101*, 6043-6047.
(7) Horn, C.; Frank, P.; Tranter, R. S.; Schaugg, J.; Grotheer, H.-H.; Just, T. Direct Measurement of the Reaction Pair $C_6H_5NO \rightarrow C_6H_5$+ NO by a Combined Shock Tube and Flow Reactor Approach. *Proc. Combust. Inst.* **1996,** *26*, 575-582.
(8) Zador, J.; Fellows, M. D.; Miller, J. A. Initiation Reactions in Acetylene Pyrolysis. *J. Phys. Chem. A* **2017,** *121*, 4203-4217.
(9) Mebel, A. M.; Landera, A.; Kaiser, R. I. Formation Mechanisms of Naphthalene and Indene: From the Interstellar Medium to Combustion Flames. *J. Phys. Chem. A* **2017,** *121*, 901-926.
(10) Mebel, A. M.; Georgievskii, Y.; Jasper, A. W.; Klippenstein, S. J. Temperature-and Pressure-Dependent Rate Coefficients for the HACA Pathways from Benzene to Naphthalene. *Proc. Combust. Inst.* **2017,** *36*, 919-926.
(11) Miller, J. A.; Klippenstein, S. J.; Robertson, S. H. A Theoretical Analysis of the Reaction Between Vinyl and Acetylene: Quantum Chemistry and Solution of the Master Equation. *J. Phys. Chem. A* **2000,** *104*, 7525-7536.
(12) Knyazev, V. D.; Slagle, I. R. Experimental and Theoretical Study of The $C_2H_3 \rightleftarrows$ H+ C_2H_2 Reaction. Tunneling and the Shape of Falloff Curves. *J. Phys. Chem.* **1996,** *100*, 16899-16911.
(13) Bauich, D.; Cobos, C.; Cox, C.; Esser, C.; Frank, P.; Just, T.; Kerr, J.; Pilling, M.; Troe, J.; Walker, R. Evaluated kinetic data for combustion modelling. *J. Phys. Chem. Ref. Data* **1992,** *21*, 411-429.
(14) Harding, L. B.; Georgievskii, Y.; Klippenstein, S. J. Predictive Theory for Hydrogen Atom− Hydrocarbon Radical Association Kinetics. *J. Phys. Chem. A* **2005,** *109*, 4646-4656.
(15) Miller, J. A.; Klippenstein, S. J. The Recombination of Propargyl Radicals and Other Reactions on a C_6H_6 Potential. *J. Phys. Chem. A* **2003,** *107*, 7783-7799.
(16) Semenikhin, A. S.; Savchenkova, A. S.; Chechet, I. V.; Matveev, S. G.; Liu, Z.; Frenklach, M.; Mebel, A. M. Rate Constants for H Abstraction from Benzo(a)pyrene and Chrysene: A Theoretical Study. *Phys. Chem. Chem. Phys.* **2017,** *19*, 25401-25413.
(17) Jasper, A. W.; Hansen, N. Hydrogen-Assisted Isomerizations of Fulvene to Benzene and of Larger Cyclic Aromatic Hydrocarbons. *Proc. Combust. Inst.* **2013,** *34*, 279-287.
(18) da Silva, G. Mystery of 1-Vinylpropargyl Formation from Acetylene Addition to the Propargyl Radical: An Open-and-Shut Case. *J. Phys. Chem. A* **2017,** *121*, 2086-2095.
(19) Madden, L. K.; Moskaleva, L. V.; Kristyan, S.; Lin, M. C. Ab Initio MO Study of the Unimolecular Decomposition of the Phenyl Radical. *J. Phys. Chem. A* **1997,** *101*, 6790-6797.
(20) Senosiain, J. P.; Miller, J. A. The Reaction of *n*-and *i*-C_4H_5 Radicals with Acetylene. *J. Phys. Chem. A* **2007,** *111*, 3740-3747.

(21) Photonionization Cross Section Database (Version 2.0), National Synchrotron Radiation Laboratory, Hefei, China, http://flame.nsrl.ustc.edu.cn/database/ (2017).